

# Effect of temperature and confining pressure on the evolution of hydraulic and heat transfer properties of geothermal fracture in granite

Biao Shu<sup>a,b,\*</sup>, Runjun Zhu<sup>a</sup>, Derek Elsworth<sup>b</sup>, Jeffrey Dick<sup>a</sup>, Shun Liu<sup>c,\*</sup>, Jingqiang Tan<sup>a</sup>, Shaohe Zhang<sup>a</sup>

<sup>a</sup> Key Laboratory of Metallogenic Prediction of Nonferrous Metals and Geological Environment Monitoring (Central South University), Ministry of Education; School of Geosciences and Info-Physics, Central South University, Changsha, Hunan 410083, PR China

<sup>b</sup> Department of Energy and Mineral Engineering, EMS Energy Institute and G3 Center, Pennsylvania State University, University Park, PA 16801, USA

<sup>c</sup> Shaanxi Key Laboratory of Advanced Stimulation Technology for Oil & Gas Reservoirs, Engineering Research Center of Development and Management for Low to Ultra-low Permeability Oil & Gas Reservoirs in West China (Ministry of Education), Xi'an Shiyou University, Xi'an, Shaanxi 710065, PR China

## HIGHLIGHTS

- Novel high temperature high confining pressure flow-through experiments and device.
- Define effect of stress and temperature on hydraulic and heat transfer properties.
- Define mechanisms of permeability and heat transfer properties evolution.
- Confining pressure impacts hydraulic response greater than heat transfer behavior.
- Temperature affects heat transfer behavior more strongly than hydraulic properties.

## ARTICLE INFO

### Keywords:

Geothermal energy  
Enhanced geothermal system  
Heat transfer coefficient  
Permeability  
Hydraulic aperture

## ABSTRACT

The hydraulic and heat transfer properties of artificial fracture networks are key to the efficiency of energy production from geothermal reservoirs. To date, no conclusive view exists of the evolution in fracture permeability and heat transfer coefficient when arbitrary stresses and temperatures are applied. This work examines the evolution of hydraulic and heat transfer properties during simulated geothermal energy extraction using a novel fluid flow-through test device accommodating large single artificial fractures in granite. Experiments are conducted in two contrasting modalities: at constant temperature with increasing confining pressures, and at constant confining pressure with increasing temperature. At constant temperature, as the confining pressure increases from 4 to 20 MPa, both hydraulic and heat transfer properties decrease, with permeability decreases by 46–63% and heat transfer coefficient decreases by 13–67%. Permeability decreases by 28–37% as temperature increases at constant confining pressure larger than 10 MPa, but permeability may first decrease and then increase at low constant confining pressure of 5 MPa. As the temperature increases from 100 to 200 °C at constant confining pressures, heat transfer coefficient increases by 25–45%. Results show that confining pressure impacts hydraulic properties more strongly than heat transfer properties, while reservoir temperature affects the heat transfer properties more strongly than hydraulic properties. These new findings on the evolution of permeability and heat transfer rate for different paths of temperature and confining pressure are critically important to the understanding of heat production from real geothermal reservoirs.

## 1. Introduction

Renewable energy can be used to reduce fossil fuel consumption and greenhouse gas emissions [1]. Geothermal energy is one promising form of renewable energy [2] that has the distinctive features of being stable and predictable as baseload power, being independent of

weather conditions [3], representing a massive reserve and being highly cost effective [1]. Current surveys show that abundant geothermal reserves exceed  $14 \times 10^{24}$  J and  $25 \times 10^{24}$  J, respectively, in the U.S. [4] and China [5].

In addition to its wide use for district heating by using ground source heat pumps (GSHP) [6], geothermal energy has also been used

\* Corresponding authors.

E-mail addresses: [biaoshu@csu.edu.cn](mailto:biaoshu@csu.edu.cn) (B. Shu), [liushun@xsyu.edu.cn](mailto:liushun@xsyu.edu.cn) (S. Liu).

## Nomenclature

### Latin alphabet

$A$	Cross sectional area of fracture [ $\text{m}^2$ ]
$A_f$	Actual fracture surface area [ $\text{m}^2$ ]
$b_e$	Equivalent hydraulic aperture [m]
$b_{ei}$	Hydraulic aperture at $i$ °C/MPa [m]
$b_{e25}$	Hydraulic aperture at 25 °C [m]
$b_{e4}$	Hydraulic aperture at 4 MPa [m]
$c$	Specific heat capacity of water [J/kg·K]
$d$	Width of the fracture (equal to the diameter of the core sample) [m]
$g$	Gravitational acceleration [ $9.8 \text{ m}^2/\text{s}$ ]
$h$	Overall heat transfer coefficient [ $\text{W}/\text{m}^2\cdot\text{K}$ ]
$h_i$	Overall heat transfer coefficient at $i$ °C/MPa [ $\text{W}/\text{m}^2\cdot\text{K}$ ]
$h_4$	Overall heat transfer coefficient at 4 MPa [ $\text{W}/\text{m}^2\cdot\text{K}$ ]
$h_{100}$	Overall heat transfer coefficient at 100 °C [ $\text{W}/\text{m}^2\cdot\text{K}$ ]
$k_e$	Permeability of fracture [ $\text{m}^2$ ]
$k_{ei}$	Permeability at $i$ °C/MPa [ $\text{m}^2$ ]
$k_{e4}$	Permeability at 4 MPa [ $\text{m}^2$ ]
$k_{e25}$	Permeability at 25 °C [ $\text{m}^2$ ]
$K$	Hydraulic conductivity [m/s]
$K_i$	Hydraulic conductivity at $i$ °C/MPa [m/s]

$K_4$	Hydraulic conductivity at 4 MPa [m/s]
$K_{25}$	Hydraulic conductivity at 25 °C [m/s]
$L$	Flow path length (equal to the length of the fracture) [m]
$P$	Water pressure difference between inlet and outlet [Pa]
$q$	Flow rate [ $\text{m}^3/\text{s}$ ]
$Q$	Heat transfer rate [J/s]
$Q_i$	Heat transfer rate at $i$ °C/MPa [J/s]
$Q_4$	Heat transfer rate at 4 MPa [J/s]
$Q_{100}$	Heat transfer rate at 100 °C [J/s]
$T$	Temperature in degrees Kelvin [K]
$T_c$	Temperature in degrees Celsius [°C]
$T_i$	Water temperature at the inlet [K]
$T_o$	Water temperature at the outlet [K]

### Greek alphabet

$\mu$	Dynamic viscosity of water [Pa·s]
$\rho$	Density of water [ $\text{kg}/\text{m}^3$ ]

### Abbreviations

EGS	Enhanced Geothermal System
GSHP	Ground source heat pumps
HDR	Hot dry rock

for electricity generation in Iceland, Kenya, Indonesia, Turkey, the United States [7]. The estimated total worldwide installed capacity of geothermal power plants was 14.3 GWe in 2017 [8]. Geothermal energy contributes ~0.3% (87 TWh) of global electricity production in 2018 [9], and this would reach ~3.5% (1400 TWh) of global electricity production [10] and avoid about 800 Mt of CO<sub>2</sub> emission per year by 2050. Therefore, geothermal power generation systems are attractive in reducing fossil fuel dependency and consumption and greenhouse gas emissions [11].

Low porosity and permeability are the common features of unconventional reservoirs [12]. It has proven a significant challenge to extract significant amounts of heat from geothermal reservoirs, due to low permeability and restricted natural heat conduction [1] in the deep reservoirs. Artificial fracture networks are usually created by hydraulic, chemical or thermal stimulation so that a heat transfer medium (such as water) can flow into the hot dry rock (HDR) reservoir and extract heat. Coupled thermal and poromechanical processes play an important role in hydraulic fracturing of geothermal reservoirs [13]. A geothermal system, with a high density of artificially created fractures, to provide conductive flow pathways, and large contact area between the flowing fluid and the surrounding rock formation [6], is required for successful Enhanced Geothermal System (EGS) production [14]. EGS, introduced in the 1970s [15], is the main sustainable and economical method to extract deep geothermal energy from HDR [16] at baseload scale.

In EGS, fluid circulation from inlet to outlet well [17] requires that the permeability of the artificial fracture network is high to maximize the energy production efficiency [18], requiring a priori assessment and quantification of anticipated permeability change during the geothermal recovery processes [19]. However, predicting the production performance is often challenging [20] because the connected fracture networks dominate the production performance in tight formations [21]. The transportation of fluid in fractures, needs further investigation [22].

Current observations typically note a reduction in permeability with increased duration of circulation [23]. As the temperature increases, the permeability of the fracture decreases [24], but the transmissivity of the fracture actually increases due to the significant decrease of the dynamic viscosity of water [25]. As the confining pressure increases,

permeability decreases due to fracture closure and aperture reduction [26].

Pressure dissolution and free-face dissolution have been implicated as two main mechanisms contributing to the permeability change. Pressure dissolution [27] is the mineral dissolution that occurs at the contacting asperities of a fracture surface; while free-face dissolution [28] is the dissolution of minerals occurring on the free fracture surface (not contacting). Permeability will reduce as mineral mass is net removed from contacting asperities [27] under pressure dissolution, and will be enhanced as free-face dissolution localizes along a solution channel [28].

As mineral elements (such as potassium, aluminum, and silicon) are dissolved during fluid flow-through in granite [29], either as free-face or pressure dissolution, minerals may later precipitate downstream on the fracture surface. Even though this mineral precipitation may be minimal, it may still impact fracture permeability [30]. In addition to mineral dissolution, mineral grains comprising fracture surface contacting asperities may be crushed under confining pressure, and the fracture aperture correspondingly reduced, due to the decrease in rock strength at high temperature [31].

To summarize, although some previous observations have explored the flow characteristics of rock fractures under high temperatures and high confining pressures, one or more shortcomings exist in these previous studies. These include, that: (1) tests were performed at relatively low temperatures, lower than 150 °C, which is typically lower than real EGS production temperatures; (2) the rock sample sizes were small, rendering it difficult to upscale results; and (3) confining pressures were small and constant. Absent are studies that change temperature and/or confining pressure during the flow-through test. To date, no conclusive view exists of the evolution of fracture permeability when arbitrary stress and temperature paths are applied [32]. Subtle changes in local conditions of applied stress or temperature may trigger switching between free-face dissolution and pressure dissolution, and therefore impact the hydraulic and heat transfer properties of fractures [32]. Therefore, there is a need to conduct further experimental studies to determine flow characteristics under arbitrary confining stress and temperature combinations.

We use a novel experimental apparatus to complete an innovative and comprehensive investigation of the effect of confining stress and

temperature paths on the evolution of hydraulic and heat transfer properties of large granite fractures. Experiments are conducted in two contrasting modalities alternately with constant temperatures and increasing confining pressures (to 20 MPa, Group A) then with constant confining pressures and increasing temperatures (to 200 °C, Group B). The test temperature and confining pressure were chosen to closely simulate the true temperature and in-situ stress of deep geothermal reservoirs. Experimental design and methods were reported for the recovery of hydraulic and heat transfer properties of hydraulic aperture, permeability, and heat transfer coefficient from the experiments. The experimental results help evaluate the heat extraction efficiency at real reservoir temperatures and in-situ stresses. This research adds a significant piece to the full picture of how fracture networks in geothermal reservoirs perform and evolve during geothermal energy production.

## 2. Experiment design

### 2.1. Fracture sample and test device

The core samples used in this study were collected from Fujian province, which is one of the most important deep geothermal reservoir areas in China. The major mineral content of this granite is 45% potassium feldspar, 25% quartz, 25% plagioclase and 5% biotite.

Granite cores were cut into cylinders 50 mm diameter and 100 mm length. A specially designed Brazilian tension test machine was used to split each cylinder into two half-cylinders along the long axis creating an artificial fracture. Fig. 1(a) shows the Brazilian tension test rig and Fig. 1(b) shows some artificially fractured samples. Laser profilometry as shown in Fig. 1(c), was used to measure the surface area of the fractures for the 8 tests in this study, which are listed in Table 1. There were totally 6 samples used in these 8 tests, as shown in Fig. 1(b). Tests

**Table 1**  
Fracture surface areas obtained from laser scanning.

Test number	#1	#2	#3	#4	#5	#6	#7	#8
Surface area ( $10^{-3} \text{ m}^2$ )	5.747	5.741	5.800	5.796	5.758	5.806	5.794	5.801

#1 and #2 used the same sample; tests #3 and #4 used another sample; tests #5, 6, 7, and 8 used the other four different samples. The fracture surface areas of tests #2 and #4 are only slightly smaller than those of tests #1 and #3, respectively.

The two half-cylinders of each sample were re-mated and wrapped in a thin layer of polymer waterproof tape before installing into a thin soft copper sleeve. The polymer tape was used to prevent water leakage from the fracture to the periphery of the core cylinder. The thin copper sleeve was used to sustain the confining pressure. Both polymer tape and the copper sleeve can withstand high temperatures. This sealing method was chosen after several trials of different sealing methods. Dye tracer tests confirmed that the water flowed only in the fracture and did not short-circuit along the periphery of the split-core.

The experimental device used in this study is a custom-designed high temperature fluid flow-through device, as shown in Fig. 2. This device can provide a confining pressure of up to 50 MPa at a test temperature of up to 350 °C. The apparatus includes a core holder, a confining pressure load unit, a pump to inject fluid into the fracture, and pressure and temperature sensors at both the inlet and outlet of the fracture. The core holder is wrapped by a heater to heat the rock sample to a designated temperature. The temperature, fluid pressure and flow rate are controlled and monitored by computer. A detailed schematic diagram of this experimental device was introduced in a previous publication [33].

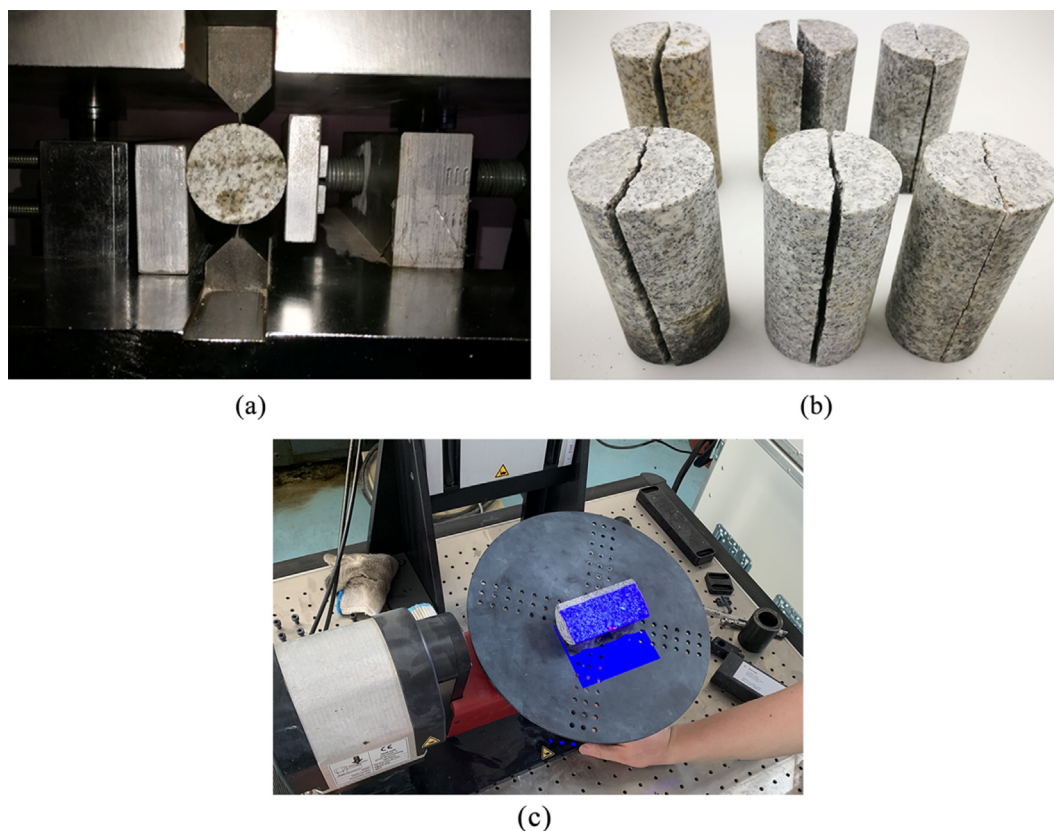


**Fig. 1.** (a) Specially designed Brazilian tension test rig used to split core cylinders; (b) some of the prepared  $\phi 50 \times 100$  mm granite samples with artificial fracture along the long axis; (c) laser profilometry to measure fracture surface area.

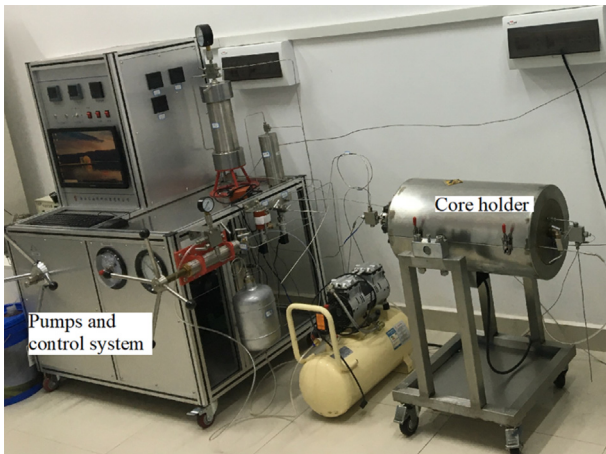


Fig. 2. Custom-designed device used for the high temperature fluid flow-through experiment.

## 2.2. Experimental procedure

The effect of confining pressure and temperature on the hydraulic and heat extraction characteristics of single fractures in granite were explored separately, using two groups of experiments.

To study the effect of changing confining pressure, in experiment group A, the temperature of the rock sample was kept constant while the confining pressure was increased from 4 MPa, in steps to 20 MPa. Group A consists of 4 individual experiments, with temperatures set to 25, 100, 150 and 200 °C, respectively. Taking the experiment at 100 °C as an example, the detailed experiment procedure is shown below:

- (1) After installing the fracture sample into the coreholder, gradually increase the sample temperature to 100 °C, at a rate of 5 °C/h;

- (2) Set the confining pressure to 4 MPa;
- (3) Inject water into the fracture to start the flow-through experiment;
- (4) After the flow rate, water pressure, and water temperature at both inlet and outlet reach stable values, record the flow rate, water temperature and water pressure at both inlet and outlet of the fracture;
- (5) Increase the confining pressure in steps to 8, 12, 16, and 20 MPa, repeating step (4) at each confining pressure.

In contrast, to study the effect of changing temperature, in experiment group B, the confining pressure was kept constant while cell and equilibrium rock temperature was stepwise incremented from 25 °C to 200 °C. Group B also consists of 4 individual experiments, with confining pressures set to 5, 10, 15 and 20 MPa, respectively. Taking the experiment at 10 MPa as an example, the detailed experimental procedure is as:

- (1) After installing the fracture sample into the coreholder, set the confining pressure to 10 MPa;
- (2) Set the sample temperature to 25 °C;
- (3) Inject water into the fracture to begin the flow-through experiment;
- (4) After the flow rate, water pressure, and water temperature at both inlet and outlet reach stable values, record the temperature and water pressure at both inlet and outlet of the fracture;
- (5) Increase the sample temperature in steps to 100, 150 and 200 °C. In order to ensure that the rock sample was thermally equilibrated, we maintained each of these three temperatures for more than 2 h before taking readings of water temperatures and pressures. Repeat step (4) at each temperature.

The highest temperature for this study is 200 °C. In order to retain the water in a liquid state, the water pressures in the fracture were kept higher than 1.62 MPa [33].

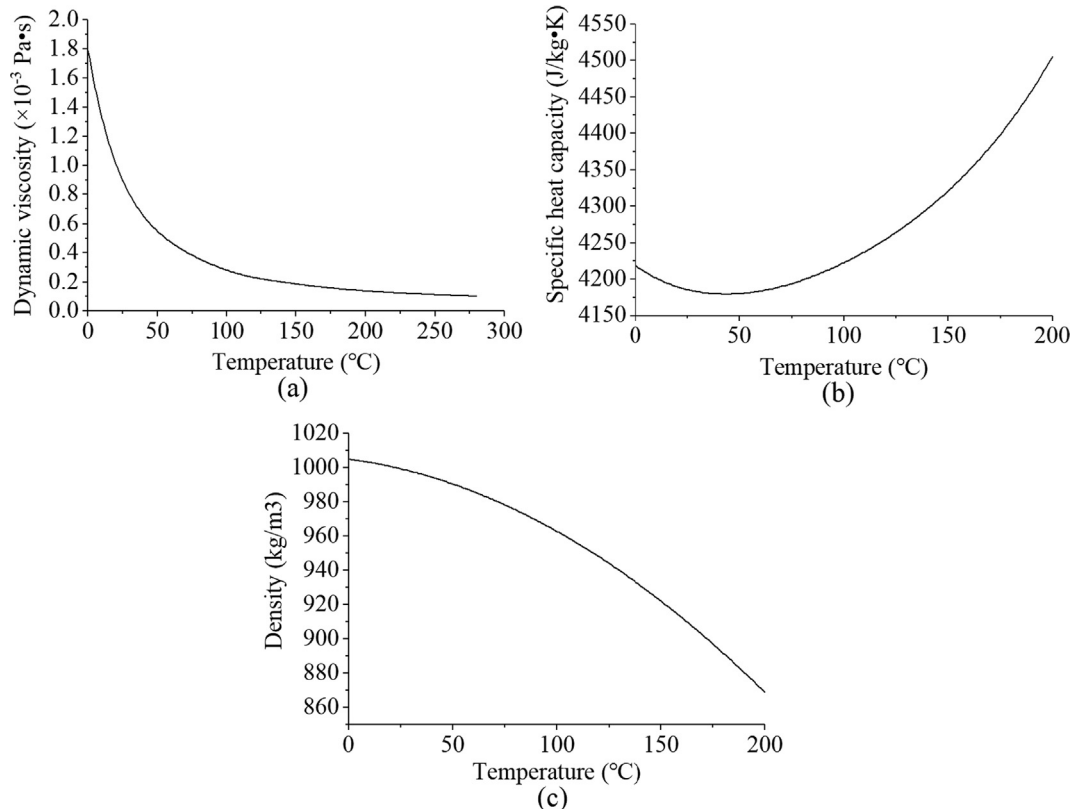


Fig. 3. Water properties over a range in temperature: (a) dynamic viscosity, (b) specific heat capacity, and (c) density.

### 3. Data reduction

#### 3.1. Hydraulic properties

To represent water flow-through a single granite fracture, the modified cubic law can be used, as shown in Eq. (1) [34]

$$q = \frac{Pdb_e^3}{12\mu L} \quad (1)$$

From Eq. (1), the equivalent hydraulic aperture  $b_e$  can be calculated.

The permeability of the single fracture was calculated according to Darcy's law [29]

$$k_e = \frac{q \cdot \mu \cdot L}{P \cdot A} \quad (2)$$

to yield

$$A = d \cdot b_e \quad (3)$$

Thus, the permeability of a single fracture can be obtained by combining Eqs. (1), (2) and (3), and is expressed as

$$k_e = \frac{b_e^2}{12} \quad (4)$$

The relationship between the dynamic viscosity of water and temperature is an important factor controlling fluid flow. The dynamic viscosity of water can be calculated using Eqs. (5) and (6) [35].

For  $273 < T < 413$  K,

$$\begin{aligned} \mu &= 1.3799 - 0.0212 \cdot T + 1.3604 \times 10^{-4} \cdot T^2 - 4.6454 \times 10^{-7} \cdot T^3 + 8.9042 \\ &\quad \times 10^{-10} \cdot T^4 - 9.0790 \times 10^{-13} \cdot T^5 + 3.8457 \times 10^{-16} \cdot T^6 \end{aligned} \quad (5)$$

For  $413 < T < 553$  K,

$$\mu = 0.0040 - 2.1074 \times 10^{-5} \cdot T + 3.8577 \times 10^{-8} \cdot T^2 - 2.3973 \times 10^{-11} \cdot T^3 \quad (6)$$

The specific heat capacity and density of water are also related to water temperature, and their relationships, for  $273 < T < 553$  K, are given as [35]

$$c = 12010 - 80.4 \cdot T + 0.3 \cdot T^2 - 5.4 \times 10^{-4} \cdot T^3 + 3.6 \times 10^{-7} \cdot T^4 \quad (7)$$

$$\rho = 838.4661 + 1.4005 \cdot T - 0.003 \cdot T^2 + 3.7182 \cdot 10^{-7} \cdot T^3 \quad (8)$$

**Table 2**

Experimental results of flow rate, water pressure and water temperature in experimental group A.

Confining pressure (MPa)		4	8	12	16	20
Test #1, 25 °C	Flow rate (ml/min)	0.37	0.33	0.25	0.20	0.19
	Water pressure at inlet (MPa)	2.77	2.84	2.91	2.97	3.00
	Water pressure at outlet (MPa)	1.99	1.99	1.99	2.00	2.00
	Water pressure difference (MPa)	0.78	0.85	0.92	0.97	1.00
	Flow rate (ml/min)	0.85	0.76	0.50	0.38	0.34
Test #2, 100 °C	Water pressure at inlet (MPa)	2.56	2.67	2.70	2.72	2.77
	Water pressure at outlet (MPa)	2.00	2.01	2.03	2.02	2.07
	Water pressure difference (MPa)	0.56	0.66	0.67	0.70	0.70
	Water temperature at inlet (°C)	90.1	90.4	90.3	90.6	90.9
	Water temperature at outlet (°C)	91.9	92.1	92.0	92.2	92.3
Test #3, 150 °C	Flow rate (ml/min)	1.00	1.00	1.00	1.00	1.00
	Water pressure at inlet (MPa)	2.13	2.40	2.67	2.83	2.99
	Water pressure at outlet (MPa)	1.90	1.95	2.04	2.07	2.09
	Water pressure difference (MPa)	0.23	0.45	0.63	0.76	0.90
	Water temperature at inlet (°C)	137.0	137.6	137.7	138.0	138.3
Test #4, 200 °C	Water temperature at outlet (°C)	139.7	140.0	140.0	140.2	140.4
	Flow rate (ml/min)	1.00	1.00	1.00	1.00	1.00
	Water pressure at inlet (MPa)	2.00	2.13	2.29	2.51	2.62
	Water pressure at outlet (MPa)	1.83	1.78	1.78	1.87	1.87
	Water pressure difference (MPa)	0.17	0.35	0.51	0.64	0.75
Water temperature at inlet (°C)		186.3	186.6	186.9	187.0	187.2
	Water temperature at outlet (°C)	189.7	189.8	189.9	189.9	190.0

The temperature may be converted between degrees Kelvin and degrees Celsius as

$$T = T_c + 273.15 \quad (9)$$

By combining Eqs. (5), (6) and (9), the dynamic viscosity of water can be calculated for different temperatures as shown in Fig. 3(a). According to Fig. 3(a), the dynamic viscosity of water decreases as temperature increases. It decreases very quickly when  $T_c < 140$  °C and slowly when  $T_c > 140$  °C.

By combining Eqs. (7), (8) and (9), the specific heat capacity and density can be calculated for different temperatures as shown in Fig. 3(b) and (c), respectively.

Hydraulic conductivity describes the flow velocity of water under unit hydraulic gradient. The larger the hydraulic conductivity, the faster the fluid flows in the fracture. The hydraulic conductivity can be calculated from

$$K = \frac{k_e \cdot g \cdot \rho}{\mu} \quad (10)$$

#### 3.2. Heat transfer properties

In order to further study the heat recovery potential of the fluid from the fracture surface, the heat that is carried out from the fracture by the water was calculated as [25]

$$Q = q\rho c(T_o - T_i) \quad (11)$$

The heat exchange characteristics between hot dry rock and water are important factors that should be included in the evaluation of HDR reservoir stimulation results and the design of EGS power plants [36]. In order to study the effect of confining pressure and temperature on the heat transfer efficiency, the concept of a heat transfer coefficient is introduced. This coefficient represents the conductive heat that is transferred between an advecting fluid medium and the surface over which the fluid flows.

The overall heat transfer coefficient is the most commonly used coefficient used to evaluate the heat transfer efficiency between hot rock and fluid. Local heat transfer coefficients are not used because the temperature distribution and the local fluid flow paths are complex and cannot be measured in flow-through test on a rough fracture.

The overall heat transfer coefficient may be measured as [37]

$$h = \frac{Q}{L \cdot d \cdot (T - 1/2(T_i + T_o))} \tag{12}$$

This may be converted by using the nominal surface area of the fracture as  $L \times d$ , since the fracture is assumed to be flat and planar. However, we are using rough fractures in this study, so  $L \times d$  should be replaced by the actual fracture surface area recovered from laser scanning of the fracture surface as listed in Table 1. Accordingly, the overall heat transfer coefficient can be calculated as

$$h = \frac{Q}{A_f \cdot (T - 1/2(T_i + T_o))} \tag{13}$$

### 4. Experimental results

#### 4.1. Results for experimental group A

In the flow-through experiments of group A, four experiments were conducted with test temperatures of 25, 100, 150, and 200 °C, respectively. In each experiment, confining pressure was increased stepwise from 4 to 8, 12, 16, and 20 MPa.

The experimental results of flow rate, water pressure at inlet and outlet and water temperature at inlet and outlet are listed in Table 2. In test #1, the rock sample and water temperature were set to 25 °C, equivalent to room temperature, so that heat transfer from the rock to the water in test #1 can be ignored. The calculated hydraulic aperture, permeability, hydraulic conductivity, heat transfer rate, and overall heat transfer coefficient are listed in Table 3.

During the experiments, the water was heated to a certain temperature in the supply lines before it reached the inlet of the fracture. For example, when the designated core temperature is 200 °C in test #4, the water temperature measured at the inlet of the fracture is ~187 °C. The water temperature continuously increased when it was flowing in the fracture, and finally reached ~190 °C at the outlet. The average temperature of the water at inlet and outlet were used to define the dynamic viscosity, density and specific heat capacity of water in the fracture.

#### 4.2. Results for experimental group B

In flow experiment for group B, four sets of experiment were conducted at confining pressures of 5, 10, 15, and 20 MPa, respectively. In each test, temperature was increased stepwise from 25 to 100, 150, and 200 °C.

**Table 3**  
Calculated hydraulic and heat transfer parameters from experimental group A.

Confining pressure (MPa)		4	8	12	16	20
Equivalent Hydraulic aperture, $b_e$ ( $\times 10^{-6}$ m)	Test #1, 25 °C	5.58	5.21	4.63	4.22	4.11
	Test #2, 100 °C	6.05	5.52	4.77	4.29	4.14
	Test #3, 150 °C	7.04	5.63	5.03	4.72	4.46
	Test #4, 200 °C	7.02	5.51	4.86	4.51	4.28
Permeability, $k_e$ ( $\times 10^{-12}$ m <sup>2</sup> )	Test #1, 25 °C	2.59	2.27	1.79	1.49	1.41
	Test #2, 100 °C	3.05	2.54	1.90	1.54	1.43
	Test #3, 150 °C	4.14	2.64	2.11	1.86	1.66
	Test #4, 200 °C	4.10	2.53	1.97	1.69	1.52
Hydraulic conductivity, $K$ ( $\times 10^{-6}$ m/s)	Test #1, 25 °C	28.33	24.80	19.54	16.26	15.40
	Test #2, 100 °C	94.24	78.65	58.82	47.74	44.44
	Test #3, 150 °C	191.87	122.72	98.06	86.56	77.35
	Test #4, 200 °C	246.75	152.43	118.56	101.90	91.66
Heat transfer rate, $Q$ (J/s)	Test #1, 25 °C	–	–	–	–	–
	Test #2, 100 °C	0.104	0.088	0.058	0.041	0.032
	Test #3, 150 °C	0.180	0.160	0.154	0.147	0.140
	Test #4, 200 °C	0.223	0.210	0.196	0.190	0.183
Overall heat transfer coefficient, $h$ (W/m <sup>2</sup> K)	Test #1, 25 °C	–	–	–	–	–
	Test #2, 100 °C	2.01	1.75	1.14	0.84	0.67
	Test #3, 150 °C	2.67	2.46	2.37	2.32	2.27
	Test #4, 200 °C	3.20	3.06	2.92	2.83	2.77

**Table 4**  
Experimental results of flow rate, water pressure and water temperature in experimental group B.

Temperature (°C)		25	100	150	200
Test #5, 5 MPa	Flow rate (ml/min)	1.00	1.00	1.00	1.00
	Water pressure at inlet (MPa)	4.16	2.68	2.52	2.10
	Water pressure at outlet (MPa)	2.13	1.93	2.13	1.85
	Water pressure difference (MPa)	2.03	0.75	0.39	0.25
	Water temperature at inlet (°C)	–	90.9	134.1	185.2
Test #6, 10 MPa	Flow rate (ml/min)	–	92.3	137.1	188.5
	Flow rate (ml/min)	1.00	1.00	1.00	1.00
	Water pressure at inlet (MPa)	3.89	2.99	2.76	2.51
	Water pressure at outlet (MPa)	1.93	1.90	2.04	1.98
	Water pressure difference (MPa)	1.96	1.09	0.72	0.53
Test #7, 15 MPa	Water temperature at inlet (°C)	–	91.1	135.2	186.1
	Water temperature at outlet (°C)	–	92.6	138.1	189.3
	Flow rate (ml/min)	1.00	1.00	1.00	1.00
	Water pressure at inlet (MPa)	5.04	3.52	3.03	2.72
	Water pressure at outlet (MPa)	1.88	1.97	1.98	1.89
Test #8, 20 MPa	Water pressure difference (MPa)	3.16	1.55	1.05	0.83
	Water temperature at inlet (°C)	–	91.3	136.9	186.8
	Water temperature at outlet (°C)	–	92.9	139.5	189.9
	Flow rate (ml/min)	1.00	1.00	1.00	1.00
	Water pressure at inlet (MPa)	3.29	2.58	2.47	2.38
Test #8, 20 MPa	Water pressure at outlet (MPa)	1.89	1.93	1.92	1.93
	Water pressure difference (MPa)	1.40	0.65	0.55	0.45
	Water temperature at inlet (°C)	–	91.5	138.2	187.8
	Water temperature at outlet (°C)	–	93.1	140.6	190.7

The experimental results of flow rate, water pressure at inlet and outlet, and water temperature at inlet and outlet are listed in Table 4. At the beginning of each test, the rock sample and water temperatures were set to 25 °C, equivalent to room temperature, so heat transfer from the rock to the water at 25 °C can be ignored. The calculated hydraulic aperture, permeability, hydraulic conductivity, heat transfer rate, and overall heat transfer coefficient are listed in Table 5.

### 5. Analysis and discussion

#### 5.1. Experimental group A

As shown in Table 3, the equivalent hydraulic aperture, permeability and hydraulic conductivity decrease substantially as the confining pressure increases at each of the four temperatures. A higher confining pressure reduces the fracture aperture and therefore results in a lower hydraulic aperture and permeability.

**Table 5**  
Calculated hydraulic and heat transfer parameters from experiment results of experimental group B.

Temperature (°C)		25	100	150	200
Hydraulic aperture, $b_e$ ( $\times 10^{-6}$ m)	Test #5, 5 MPa	5.71	5.49	5.94	6.18
	Test #6, 10 MPa	5.75	4.85	4.83	4.80
	Test #7, 15 MPa	4.88	4.30	4.25	4.13
	Test #8, 20 MPa	6.38	5.75	5.26	5.06
Permeability, $k_e$ ( $\times 10^{-12}$ m <sup>2</sup> )	Test #5, 5 MPa	2.72	2.52	2.94	3.18
	Test #6, 10 MPa	2.76	1.96	1.95	1.92
	Test #7, 15 MPa	1.98	1.54	1.50	1.42
	Test #8, 20 MPa	3.39	2.75	2.30	2.13
Hydraulic conductivity, $K$ ( $\times 10^{-6}$ m/s)	Test #5, 5 MPa	28.76	78.33	134.50	190.74
	Test #6, 10 MPa	29.56	61.10	89.49	115.64
	Test #7, 15 MPa	21.61	48.36	69.71	85.78
	Test #8, 20 MPa	37.32	86.37	107.42	129.06
Heat transfer rate, $Q$ (J/s)	Test #5, 5 MPa	–	0.095	0.200	0.216
	Test #6, 10 MPa	–	0.102	0.194	0.210
	Test #7, 15 MPa	–	0.109	0.174	0.203
	Test #8, 20 MPa	–	0.109	0.160	0.190
Overall heat transfer coefficient, $h$ (W/m <sup>2</sup> K)	Test #5, 5 MPa	–	1.97	2.42	2.85
	Test #6, 10 MPa	–	2.15	2.42	2.85
	Test #7, 15 MPa	–	2.38	2.54	3.01
	Test #8, 20 MPa	–	2.43	2.60	3.04

From Table 3, we observe that the magnitudes of reduction in hydraulic properties change with temperature as the confining pressure increases. Generally, the higher the temperature, the larger the reduction in hydraulic aperture.

It is not appropriate to compare the hydraulic and heat transfer properties between different tests in Table 3 because the rock samples are different in each test. Therefore, in order to compare the sensitivity of confining pressure to the hydraulic parameters under different temperatures, the ratios of hydraulic aperture, permeability, and

hydraulic conductivity, relative to initial conditions (4 MPa), are calculated and shown in Fig. 4.

In Fig. 4, the curves of hydraulic aperture and permeability present the same shape, but the decrease rate of permeability is much higher than that of hydraulic aperture. With confining pressure increases from 4 to 20 MPa, hydraulic aperture decreases by 26%, 32%, 37%, and 39%, while both permeability and hydraulic conductivity decrease by 46%, 53%, 60% and 63%, at temperatures of 25, 100, 150, and 200 °C, respectively. From Fig. 4, we observe that the ratios of hydraulic

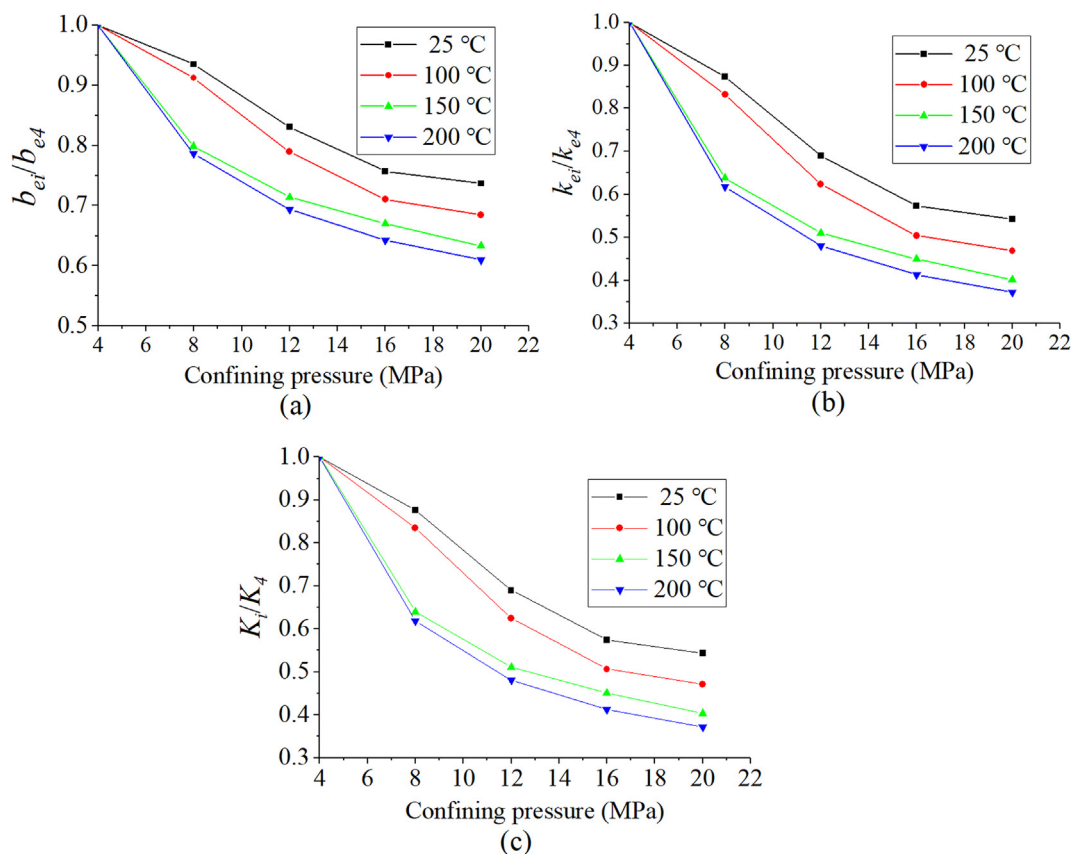


**Fig. 4.** Ratios of (a) hydraulic aperture; (b) permeability; and (c) hydraulic conductivity as a function of confining pressure normalized to 4 MPa in experimental group A.

aperture, permeability, and hydraulic conductivity decrease more rapidly at high temperatures than those at lower temperatures. The reason for the greater decrease in hydraulic properties of single fractures with an increase in temperature may be explained by two mechanisms.

First, we can consider the decrease in elastic modulus of the rock matrix. As the temperature increases, the elastic modulus of the granite decreases [38], so under the same confining pressure, the deformation of the fracture-propping asperities is larger – resulting in a greater decrease in fracture aperture. A second reason is due to the development of micro-cracks between mineral grains within the matrix. Because micro-cracks between mineral grains may be induced as the temperature increases [38], the mineral grains may rupture under increasing confining pressure and high temperature. These two processes are additive, one reversible and one irreversible, and are illustrated in Fig. 5. The dashed line represents the fracture surface before deformation. In our study, the influent water temperature is only slightly lower than the rock temperature. For example, in Table 2, the influent water temperatures are greater than 90, 140, and 185 °C when rock temperatures are 100, 150, and 200 °C, respectively. The temperature difference between water and rock is small, and therefore the induced thermal stress may also be ignored.

We note that previous studies have considered free-face dissolution and pressure dissolution as the main reason for an observed decrease of hydraulic aperture [28]. However, in our experiments from group A, the confining pressure was increased over only a few minutes, with each experiment lasting a maximum of 1–2 h. Therefore, there is likely insufficient time for significant free face dissolution or pressure dissolution to evolve. From Fig. 5, we can see that there are only elastic deformation and few mineral grains break off occurred at fracture surface in experimental group A, and there is basically no mineral dissolution involved. Besides, we can see from Table 1 that the fracture surface areas of tests #2 and #4 are only slightly smaller than those of tests #1 and #2, respectively, which means little damage occurred to the fracture surfaces. Therefore, the rock samples used in tests #1 and #3 can be reused in tests #2 and #4, respectively.

The heat transfer properties can be represented by the heat transfer rate and overall heat transfer coefficient. In order to explore the change of heat transfer properties at different temperatures, we compared the ratios of decrease in heat transfer rate and overall heat transfer coefficient, as shown in Fig. 6.

When the rock temperature was set to room temperature (25 °C), the rock and influent water temperatures were near identical, and heat transfer between water and rock can be ignored – thus, only heat transfer at temperatures of 100, 150, and 200 °C were calculated.

From Fig. 6, we note that the heat transfer rate  $Q$  and overall heat transfer coefficient  $h$  at 100 °C decrease by 69% and 67%, respectively, as the confining pressure increases from 4 MPa to 20 MPa. However, they decrease by only 22% and 15% at 150 °C, and 18% and 13% at 200 °C.

Overall, the heat transfer properties are more sensitive to confining pressure when temperature is low (100 °C), while the sensitivity decreases when temperature is high (150 and 200 °C). Therefore, the higher the geothermal reservoir temperature, the more likely that the heat transfer properties will be stable. It should be noted that we cannot compare the heat transfer properties at different temperatures, because the tests were conducted in different rock samples.

After comparing changes in hydraulic conductivity and heat transfer at 150 and 200 °C, we find that an increase in confining pressure affects the hydraulic properties more than it affects the heat transfer properties.

## 5.2. Experimental group B

In order to compare the sensitivity to temperature of the hydraulic parameters at different confining pressures, the ratios of hydraulic

aperture, permeability and hydraulic conductivity are calculated from Table 5 and shown in Fig. 7.

From Fig. 7, we observe that as the temperature increases, the calculated hydraulic aperture and permeability generally decrease, but the hydraulic conductivity  $K$  increases. From Eq. (10), we observe that the hydraulic conductivity  $K$  is proportional to the permeability  $k_e$  and water density  $\rho$ , but it is inversely proportional to the dynamic viscosity  $\mu$  of water. The decrease in dynamic viscosity is much greater than the decrease in permeability and density, and therefore, the hydraulic conductivity eventually increases. For example, for a confining pressure of 20 MPa in Fig. 7, as temperature increases from 25 to 200 °C,  $k_e$  decreases from  $3.39 \times 10^{-12}$  to  $2.13 \times 10^{-12}$  m<sup>2</sup>. From Fig. 3, we also know that  $\rho$  decreases from 999.2 to 868.9 kg/m<sup>3</sup>, and  $\mu$  decreases from  $8.93 \times 10^{-4}$  to  $1.38 \times 10^{-4}$  Pa·s. We calculate hydraulic conductivity  $K$  using Eq. (10) and find that it increases from  $37.32 \times 10^{-6}$  to  $129.06 \times 10^{-6}$  m/s.

We also observe that at a confining pressure of 5.0 MPa, the hydraulic aperture and permeability fluctuates as the temperature increases. Permeability first decreases by 7% as temperature increases from 25 to 100 °C, and then it increases by 8% and 17% as temperature continues to increase to 150 and 200 °C, respectively. This may occur because the confining pressure of 5.0 MPa is not significantly larger than the fluid pressure in the fracture. At low confining pressure, even though the elastic modulus of the rock decreases as the temperature increases, the confining pressure is insufficiently large to tightly close

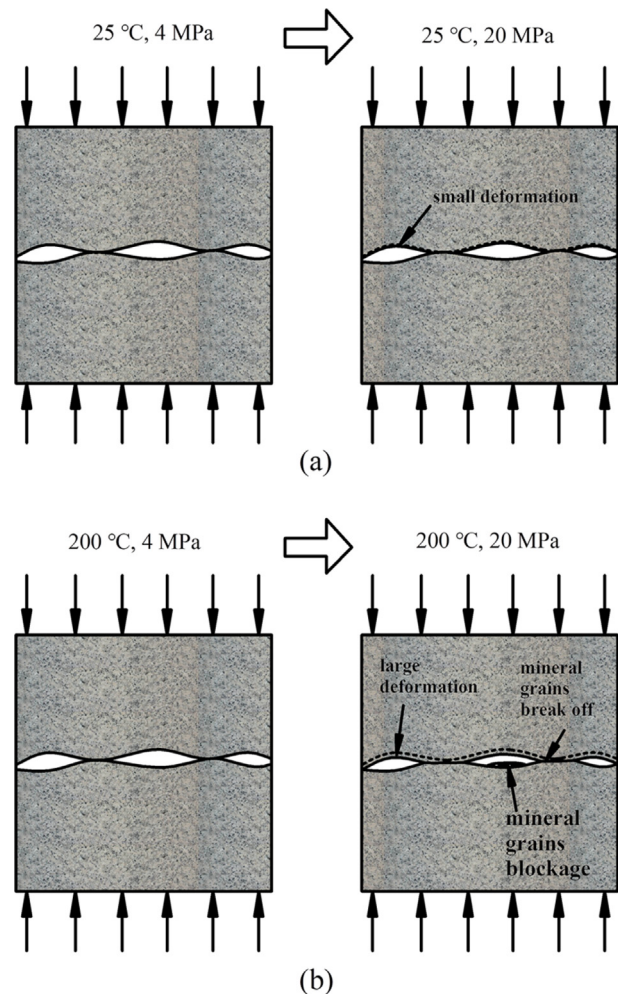


Fig. 5. Schematic explanation of the different rates of decrease in hydraulic properties: (a) low temperature (e.g. 25 °C); (b) high temperature (e.g. 200 °C). The dash line represents the fracture surface before the deformation.

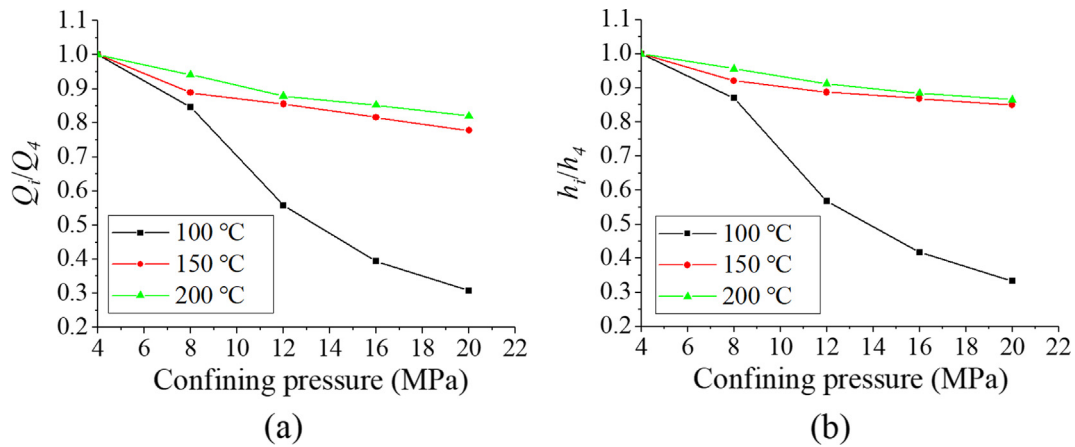


Fig. 6. Ratios of (a) heat transfer rate and (b) overall heat transfer coefficient of granite fractures at different confining pressures normalized to 4 MPa in experimental group A.

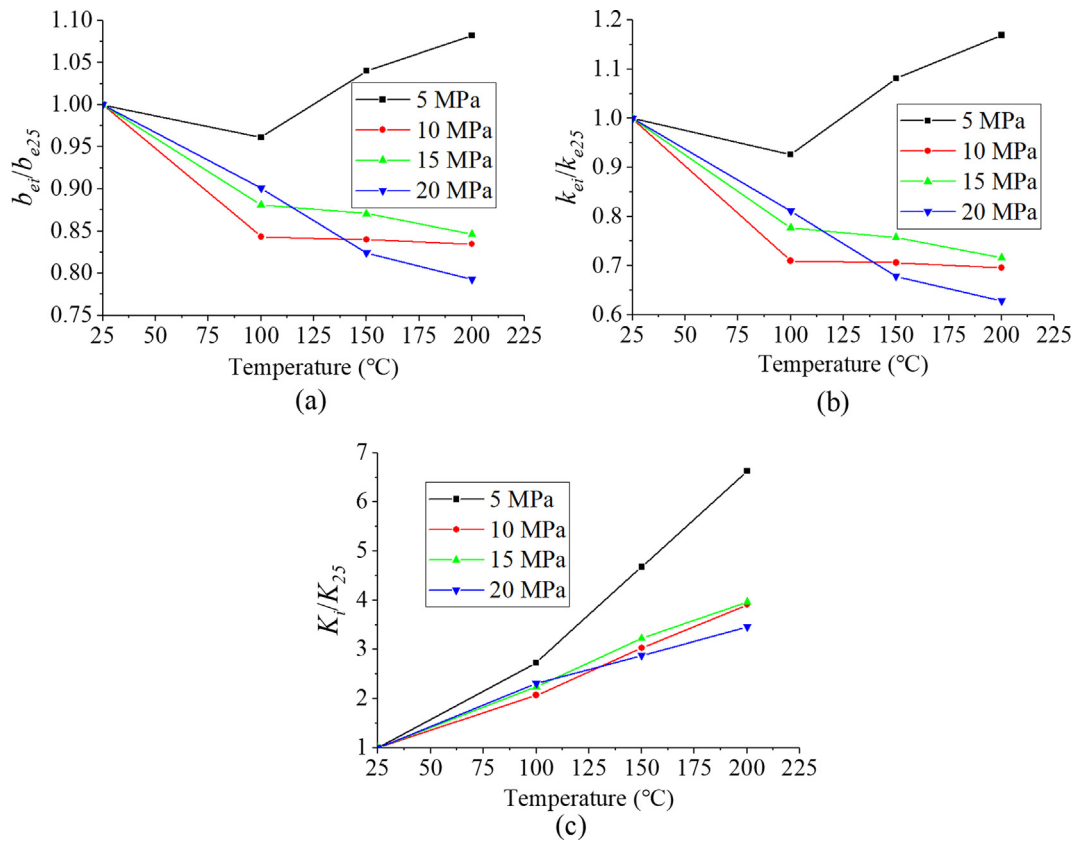


Fig. 7. Ratios of (a) hydraulic aperture, (b) permeability and (c) hydraulic conductivity at different temperatures normalized to 25 °C in experimental group B.

the fracture. Supporting asperities on the fracture surface would not be crushed under such a low confining pressure, so the hydraulic aperture changes little. Conversely, we note that in experimental group B, in order to ensure that the rock sample was completely heated, we maintained each temperature (100, 150, and 200 °C) for more than 2 h, thereby making each test ~6 h in duration. During these several hours, free face dissolution may have occurred. However, conversely, pressure solution may potentially be ignored due to the low confining pressure. Therefore, the fracture aperture may be increased. This explanation for the permeability change is illustrated in Fig. 8(a). These findings are consistent with those of Polak et al. [27] and Liu et al. [28]: that permeability enhancement is caused by free-face dissolution localized along a solution channel.

At confining pressures of 10, 15, and 20 MPa, there are clear trends

illustrating that the hydraulic aperture decreases. Permeability decreases by 30%, 28%, and 37% at confining pressures of 10, 15, and 20 MPa, respectively. Several causes may contribute to this effect.

First, under high confining pressure, the contacting asperities supporting the fracture surfaces experience more deformation due to a decrease in elastic modulus at high temperature. Secondly, some of the contact points may be crushed at high confining pressure, due to a decrease in the bond strength of mineral grains at elevated temperature. At the same time, the crushed granite particles may block the path of fluid flow, and therefore reduce the hydraulic aperture of the fracture. Finally, at high confining pressures (such as 10, 15, and 20 MPa), pressure dissolution of prograde minerals is more notable than at low confining pressure (such as 5 MPa). Thus, permeability is reduced as net mineral mass is removed from the contacting asperities (pressure

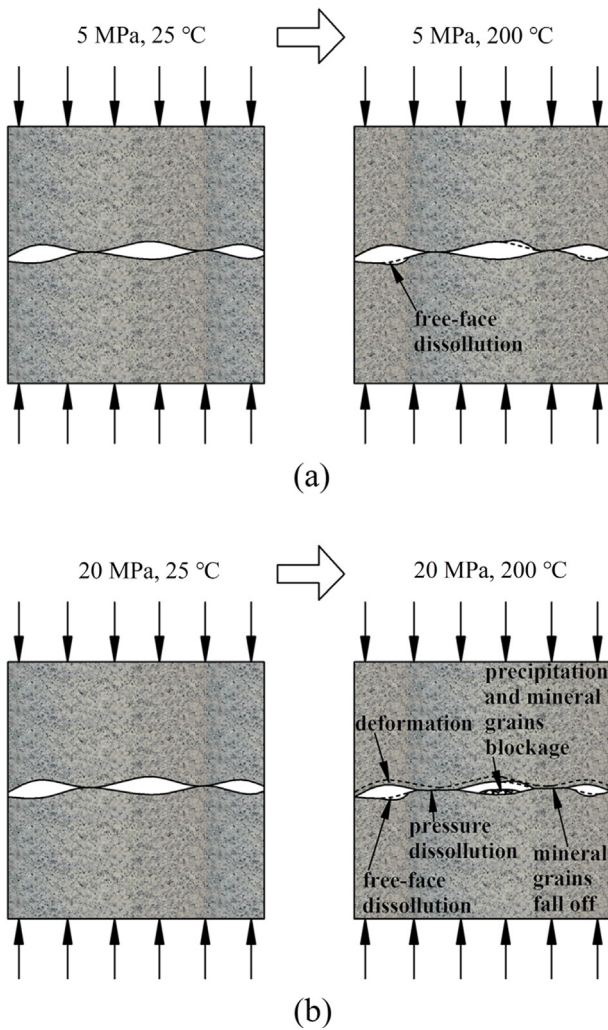


Fig. 8. Explanation of changes in fracture aperture observed in experimental group B: (a) low confining pressure (5 MPa); (b) high confining pressure (e.g. 20 MPa). The dash line represents the fracture surface before the deformation or the free face dissolution.

dissolution), and more dissolution causes more precipitation of chemical components on the fracture surface and further reduces the fracture aperture. These explanations for how the fracture aperture and permeability change are illustrated in Fig. 8(b). Due to the involvement of strong mineral dissolution, some types of minerals may dissolved more

than other types and fracture surface can be seriously changed/damaged. Reusing sample may cause misleading experimental results, therefore, no samples were reused in experimental group B.

The ratios of heat transfer rate and overall heat transfer coefficient are calculated and shown in Fig. 9. As mentioned above, the heat transfer between water and rock at a test temperature of 25 °C is null, so only the heat transfer responses at 100, 150, and 200 °C were calculated.

From Fig. 9, we observe that both heat transfer rate and overall heat transfer coefficient increase as temperature increases. At all four confining pressures, the change of heat transfer properties is indeed systematic, compared to the non-systematic change ratios of hydraulic properties. With temperature increases from 100 to 200 °C, heat transfer rate increases by 127%, 106%, 86%, and 74%, while overall heat transfer coefficient increases by 45%, 36%, 27%, and 25%, at confining pressures of 5, 10, 15, and 20 MPa, respectively. Overall, the lower the confining pressure, the more the heat transfer rate and overall heat transfer coefficient increase. The heat transfer rate increases more slowly as the temperature increases; but the overall heat transfer coefficient increases more rapidly as the temperature increases.

From Eq. (11), we observe that heat transfer rate is directly proportional to the flow rate  $q$ , water density  $\rho$ , specific heat capacity  $c$ , and the water temperature difference between outlet and inlet ( $T_o - T_i$ ). From Table 4, the flow rates in experimental group B are all the same (1.0 ml/min). From Fig. 3, we see that water density decreases, while specific heat capacity increases, with an increase in temperature. However, the product of the density and specific heat capacity of water at 100 °C is only 1.038 times of that at 200 °C. Therefore, the change in heat transfer rate is mainly caused by the difference in water temperature between inlet and outlet.

The water temperature difference increases as the test temperature increases. Therefore, in total, the heat transfer rate increases with the combination of all these factors. In addition, the change in heat transfer coefficient is mainly caused by the change in heat transfer rate.

The confining stress exerts significant impact on heat transfer properties when temperature is 100 °C. However, at EGS reservoir temperatures (greater than 150 °C), there is no significant difference between the water temperature differences at different confining pressures. Thus, confining pressure is not a major factor affecting heat transfer during EGS geothermal production, but the reservoir temperature is.

After comparing the changes in hydraulic conductivity and in heat transfer at 10, 15 and 20 MPa, we observe that the increase in temperatures influence the heat transfer properties more than they influence the hydraulic properties.

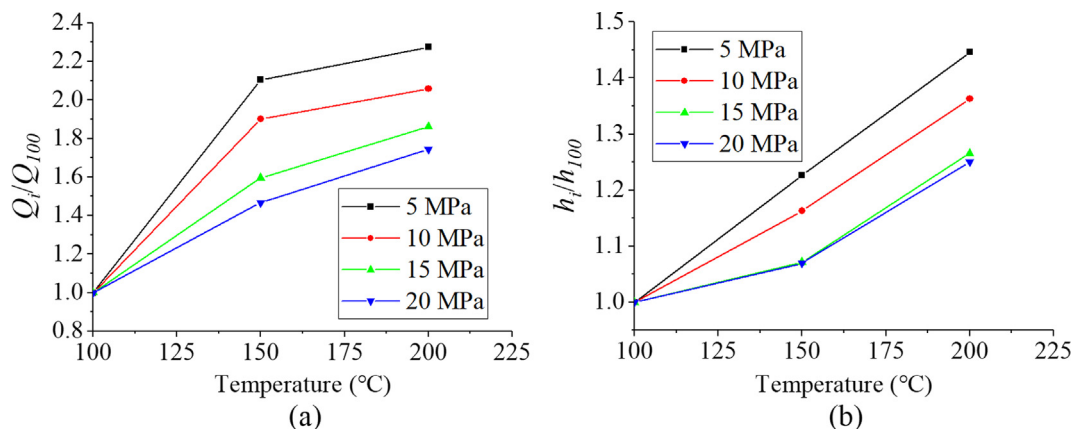


Fig. 9. Heat transfer properties increase at different temperatures with constant confining pressures. Ratios of: (a) heat transfer rate; (b) overall heat transfer coefficient at different temperatures normalized to 100 °C in experimental group B.

## 6. Conclusion

We report fluid flow-through experiments on single fractures in granite at different temperatures and confining pressures, to explore the effect of confining pressure and temperature changes on permeability and heat transfer properties. Experiments are conducted in two contrasting modalities: at constant temperature with increasing confining pressures, and at constant confining pressure with increasing temperature. The main conclusions can be summarized as follows:

- (1) At constant temperature, as the confining pressure increases, the hydraulic aperture, permeability and conductivity decrease rapidly. This is due to the high confining pressure acting on the low stiffness fracture. The higher the constant temperature, the larger the drop in hydraulic properties. This is because the high temperature decreases the elastic modulus of the granite, so that the fracture can close more tightly.
- (2) At low constant confining pressure (e.g. 5 MPa), as the temperature increases, the hydraulic aperture and permeability eventually increase. This is because at low confining pressure, free-face dissolution occurs on the fracture faces resulting in aperture increase, while the impacts of pressure dissolution may be ignored. At high constant confining pressure (e.g. greater than 10 MPa), the hydraulic aperture and permeability decrease rapidly with increase in temperature. This is due to a decrease in either elastic modulus or bond strength of the mineral grains, pressure dissolution at contacting asperities, or a combination of these effects.
- (3) At constant temperature, heat transfer rate and overall heat transfer coefficient both decrease as confining pressure increases. The heat transfer properties are highly sensitive to confining pressure at low temperatures (100 °C), while the sensitivity decreases at higher temperature (e.g. 150 and 200 °C).
- (4) At constant confining pressures, heat transfer properties consistently increase as the temperature increases. This may result mainly from the increasing water temperature difference between inlet and outlet, as rock temperature increases. The lower the confining pressure, the larger the heat transfer rate and overall heat transfer coefficient both increase.
- (5) Combining the results of the two groups of experiments, under temperatures typical of Enhanced Geothermal Systems, we conclude that confining pressure is the main factor controlling the hydraulic properties, and reservoir temperature is the main factor controlling heat transfer properties.
- (6) Observations at relatively low temperature (e.g. 100 °C), or at low confining pressure (e.g. 5 MPa), are significantly different from those obtained at high temperature (e.g. 150 and 200 °C), or high confining pressure (e.g. greater than 10 MPa). Our observations at both high confining pressures and high temperature are more applicable to the environment characteristic of real Enhanced Geothermal Systems.

## CRedit authorship contribution statement

**Biao Shu:** Conceptualization, Methodology, Resources, Writing - original draft, Visualization, Supervision, Funding acquisition. **Runjun Zhu:** Formal analysis, Investigation, Writing - original draft. **Derek Elsworth:** Formal analysis, Writing - review & editing. **Jeffrey Dick:** Writing - review & editing. **Shun Liu:** Methodology, Resources, Writing - review & editing. **Jingqiang Tan:** Methodology. **Shaoh Zhang:** Resources, Project administration.

## Acknowledgement

This research was funded by National Natural Science Foundation of China (No. 41702387) and China Scholarship Council (No. 201806375026).

## References

- [1] Liu Q, Shang LL, Duan YY. Performance analyses of a hybrid geothermal-fossil power generation system using low-enthalpy geothermal resources. *Appl Energy* 2014;162:149–62.
- [2] Cui GD, Ren SR, Rui ZH, Ezekiel J, Zhang L, Wang HS. The influence of complicated fluid-rock interactions on the geothermal exploitation in the CO<sub>2</sub> plume geothermal system. *Appl Energy* 2018;227:49–63.
- [3] Cui G, Zhang L, Ren B, Enechukwu C, Liu YM, Ren SR. Geothermal exploitation from depleted high temperature gas reservoirs via recycling supercritical CO<sub>2</sub>: heat mining rate and salt precipitation effects. *Appl Energy* 2016;183:837–52.
- [4] Tester JW, Anderson BJ, Batchelor AS, Blackwell DD, DiPippo R, Drake EM, et al. The future of geothermal energy: Impact of enhanced geothermal systems (EGS) on the United States in the 21st century. Massachusetts Institute of Technology; 2006.
- [5] Wang G, Li K, Wen D, Lin WJ, Lin LJ, Liu ZM, et al. Assessment of geothermal resources in China. In: Thirty-eighth workshop on geothermal reservoir engineering, Stanford University; 2013. p. 11–13.
- [6] Wu BS, Zhang X, Jeffrey RG, Bunker AP, Jia SP. A simplified model for heat extraction by circulating fluid through a closed-loop multiple-fracture enhanced geothermal system. *Appl Energy* 2016;183:1664–81.
- [7] Song XZ, Shi Y, Li GS, Yang RY, Wang GS, Zheng R, et al. Numerical simulation of heat extraction performance in enhanced geothermal system with multilateral wells. *Appl Energy* 2018;218:325–37.
- [8] Pan SY, Gao MY, Shah KJ, Zheng JM, Pei SL, Chiang PC. Establishment of enhanced geothermal energy utilization plans: barriers and strategies. *Renew Energy* 2019;132:19–32.
- [9] IEA. World Energy Outlook 2018. Paris: International Energy Agency; 2018.
- [10] IEA. Technology Roadmap-Geothermal Heat and Power. Paris, France: International Energy Agency; 2011.
- [11] Shu B, Zhu RJ, Zhang SH, Dick J. A qualitative prediction method of new crack-initiation direction during hydraulic fracturing of pre-cracks based on hyperbolic failure envelope. *Appl Energy* 2019;248:185–95.
- [12] Zhou DS, Zheng P, Yang JW, Li M, Xia YC, Cai WB, et al. Optimizing the construction parameters of modified zipper fracs in multiple horizontal wells. *J Nat Gas Sci Eng* 2019;71:102966.
- [13] Ezzat M, Ezzat S. Fractional thermoelasticity applications for porous asphaltic materials. *Pet Sci* 2016;13(3):550–60.
- [14] Hofmann H, Babadagli T, Zimmermann G. Hot water generation for oil sands processing from enhanced geothermal systems: process simulation for different hydraulic fracturing scenarios. *Appl Energy* 2014;113:524–47.
- [15] Olasolo P, Juárez MC, Morales MP, D'Amico S, Liarte IA. Enhanced geothermal systems (EGS): a review. *Renew Sustain Energy Rev* 2016;56:133–44.
- [16] Anderson A, Rezaie B. Geothermal technology: trends and potential role in a sustainable future. *Appl Energy* 2019;248:18–34.
- [17] White M, Fu PC, McClure M, Danko G, Elsworth D, Sonnenthal E, et al. A suite of benchmark and challenge problems for enhanced geothermal systems. *Geomech Geophys Geo-energy Geo-Resour* 2018;4(1):79–117.
- [18] Zhong Z, Elsworth D, Hu YJ. Evolution of strength and permeability in stressed fractures with fluid-rock interactions. *Pure Appl Geophys* 2016;173:525–36.
- [19] Yasuhara H, Polak A, Mitani Y, Grader AS, Halleck PM, Elsworth D. Evolution of fracture permeability through fluid-rock reaction under hydrothermal conditions. *Earth Planet Sci Lett* 2006;244(1):186–200.
- [20] Liu S, Zhang LM, Zhang K, Zhou JR, He H, Hou ZW. A simplified and efficient method for water flooding production index calculations in low permeable fractured reservoir. *J Energy Res Technol* 2019;141(11):112905.
- [21] He YW, Cheng SQ, Sun Z, Chai Z, Rui ZH. Improving oil recovery through fracture injection and production of multiple fractured horizontal wells. *J Energy Res Technol* 2020;142(5):053002.
- [22] Liu S, Wang JJ, He H, Wang H. Mechanism on imbibition of fracturing fluid in nanopore. *Nonosci Nanotechnol Lett* 2018;10(1):87–93.
- [23] Morrow CA, Moore DE, Lockner DA. Permeability reduction in granite under hydrothermal conditions. *J Geophys Res Solid Earth* 2001;106(B12):30551–60.
- [24] Polak A, Elsworth D, Yasuhara H, Grader AS, Halleck PM. Permeability reduction of a natural fracture under net dissolution by hydrothermal fluids. *Geophys Res Lett* 2003;30(20):2020.
- [25] Luo J, Zhu Y, Guo Q, Tan L, Zhuang YQ, Liu ML, et al. Experimental investigation of the hydraulic and heat transfer properties of artificially fractured granite. *Sci Rep* 2017;7:39882.
- [26] Yasuhara H, Elsworth D. Evolution of permeability in a natural fracture: significant role of pressure solution. *J Geophys Res* 2004;109:B03204.
- [27] Polak A, Elsworth D, Liu JS, Grader AS. Spontaneous switching of permeability changes in a limestone fracture with net dissolution. *Water Resour Res* 2004;40:W035502.
- [28] Liu JS, Sheng JC, Polak A, Elsworth D, Yasuhara H, Grader AS. A fully-coupled hydrological-mechanical-chemical model for fracture sealing and preferential opening. *Int J Rock Mech Min Sci* 2006;43:23–36.
- [29] Caulk RA, Ghazanfari E, Perdrial JN, Perdrial N. Experimental investigation of fracture aperture and permeability change within Enhanced Geothermal Systems. *Geothermics* 2016;62:12–21.
- [30] Yasuhara H, Kinoshita N, Ohfuji H, Lee DS, Nakashima S, Kishida K. Temporal alteration of fracture permeability in granite under hydrothermal conditions and its interpretation by coupled chemo-mechanical model. *Appl Geochem* 2011;26(12):2074–88.
- [31] Siratovich PA, Villeneuve MC, Cole JW, Kennedy BM, Bégoué F. Saturated heating and quenching of three crustal rocks and implications for thermal stimulation of

- permeability in geothermal reservoirs. *Int J Rock Mech Min Sci* 2015;80:265–80.
- [32] Yuan B, Wood DA. A holistic review of geosystem damage during unconventional oil, gas and geothermal energy recovery. *Fuel* 2018;227:99–110.
- [33] Shu B, Zhu RJ, Tan JQ, Zhang SH, Liang M. Evolution of permeability in a single granite fracture at high temperature. *Fuel* 2019;242:12–22.
- [34] Witherspoon PA, Wang JSY, Iwai K, Gale JE. Validity of cubic law for fluid flow in a deformable rock fracture. *Water Resour Res* 1980;16(6):1016–24.
- [35] Qu ZQ, Zhang W, Guo TK. Influence of different fracture morphology on heat mining performance of enhanced geothermal systems based on COMSOL. *Int J Hydrogen Energy* 2017;42(29):18263–78.
- [36] Ogino F, Yamamura M, Fukuda T. Heat transfer from hot dry rock to water flowing through a circular fracture. *Geothermics* 1999;28:21–44.
- [37] Bai B, He Y, Li X, Li J, Huang XX, Zhu JL. Experimental and analytical study of the overall heat transfer coefficient of water flowing through a single fracture in a granite core. *Appl Therm Eng* 2017;116:79–90.
- [38] Zhou XP, Li GQ, Ma HC. Real-time experiment investigations on the coupled thermomechanical and cracking behaviors in granite containing three pre-existing fissures. *Eng Fract Mech* 2020;224:106797.